# Coexistence of a Two-States Organization for a Cell-Penetrating Peptide in Lipid Bilayer

Thomas Plénat, Sylvie Boichot, Patrice Dosset, Pierre-Emmanuel Milhiet, and Christian Le Grimellec
Nanostructures et Complexes Membranaires, Centre de Biochimie Structurale, INSERM UMR 554, CNRS UMR 5048-Université Montpellier I, 34090 Montpellier Cedex, France

ABSTRACT Primary amphipathic cell-penetrating peptides transport cargoes across cell membranes with high efficiency and low lytic activity. These primary amphipathic peptides were previously shown to form aggregates or supramolecular structures in mixed lipid-peptide monolayers, but their behavior in lipid bilayers remains to be characterized. Using atomic force microscopy, we have examined the interactions of $P_{(\alpha)}$, a primary amphipathic cell-penetrating peptide which remains $\alpha$-helical whatever the environment, with dipalmitoylphosphatidylcholine (DPPC) bilayers. Addition of $P_{(\alpha)}$ at concentrations up to 5 mol % markedly modified the supported bilayers topography. Long and thin filaments lying flat at the membrane surface coexisted with deeply embedded peptides which induced a local thinning of the bilayer. On the other hand, addition of $P_{(\alpha)}$ only exerted very limited effects on the corresponding liposome's bilayer physical state, as estimated from differential scanning calorimetry and diphenylhexatriene fluorescence anisotropy experiments. The use of a gel-fluid phase separated supported bilayers made of a dioleoylphosphatidylcholine/dipalmitoylphosphatidylcholine mixture confirmed both the existence of long filaments, which at low peptide concentration were preferentially localized in the fluid phase domains and the membrane disorganizing effects of 5 mol % $P_{(\alpha)}$. The simultaneous two-states organization of $P_{(\alpha)}$, at the membrane surface and deeply embedded in the bilayer, may be involved in the transmembrane carrier function of this primary amphipathic peptide.

## INTRODUCTION

Cell membrane carrier peptides, also called cell-penetrating peptides (CPPs) are natural or synthetic water soluble peptides that translocate cell membranes with high efficiency and low lytic activity. Because they have successfully been used for the efficient intracellular delivery of large hydrophilic molecules like oligonucleotides and proteins (1), CPPs have emerged as promising tools in drug delivery (1–4). However the mechanisms involved in the CPP-cargo translocation across the cells plasma membrane remain a matter of debate. Thus, whereas receptor-mediated process can be excluded, it is not clear to what extent some of the CPPs require energy to enter the cell (5–7). Interactions between CPPs and membrane lipids are likely to play a major role in the translocation processes, even if peptide-lipid interactions alone cannot explain the different cellular uptake characteristics exhibited by these peptides (8). So far, most peptide-lipid interaction studies have focused on penetratin, the pAntp peptide, corresponding to residues 43–58 of the homeodomain of Antennapedia. Different CPP-cargo translocation mechanisms have been hypothesized: an inverted micelle mechanism (2,3), more recently an electroporation-like permeabilization mechanism (9), or both (10).

The family of primary amphipathic CPPs was designed hypothesizing that the vector peptides must contain both a hydrophobic sequence for membrane binding and a hydrophilic sequence bearing a signal targeting a subcellular compartment (11–13). Primary amphipathic CPPs bearing the nuclear localization sequence (NLS) of SV40 large T antigen (14,15) at their C-terminal and either the signal peptide of the Ig (V) light chain of caiman crocodylus (SP-NLS) (16) or a derivative of the fusion sequence of HIV1 gp41 protein (17) as the hydrophobic sequences (FP-NLS) were shown to deliver oligonucleotides into mammalian cells independently of the endosome pathway (18). Both SP-NLSs and FP-NLSs are nonstructured in water, whereas their hydrophobic domain is $\alpha$-helical in the presence of trifluoroethanol or in sodium dodecycl sulfate micelles (16,19). Studies on lipid-peptide interactions in monolayers using isotherms, circular dichroism, and Fourier transform infrared analysis showed that, as a function of the molar fraction and of the phospholipid used, SP-NLS primary amphipathic CPPs can undergo an $\alpha$- to $\beta$-conformational transition (20,21). Recently, a primary amphipathic CPP derived from the FP-NLS peptide with the sequence GALFLAFLAAALSLMGLWSQPKKKRKV, called thereafter $P_{(\alpha)}$, was synthesized. This peptide remains $\alpha$-helical whatever its environment (22). In Langmuir-Blodgett (LB) monolayers, atomic force microscopy (AFM) data in air demonstrated that $P_{(\alpha)}$ distribution is not homogeneous. It forms aggregates or supramolecular structures of variable size and shape according to the peptide concentration and the lipid used (22,23), like the other members of the primary amphipathic CPP family (16,17). In addition, these mesoscopic structures often coexist with a liquid-expanded phase composed of miscible peptide lipid (23).

To further characterize the primary amphipathic CPP interactions with membranes, we have examined, by AFM under aqueous conditions, the behavior of $P_{(\alpha)}$ in bilayers.

*Submitted February 23, 2005, and accepted for publication July 18, 2005.*

Address reprint requests to Christian Le Grimellec, Nanostructures et Complexes Membranaires, CBS, INSERM UMR 554, 29 rue de Navacelles, 34090 Montpellier Cedex, France. Tel.: 33-467-41-79-07; Fax: 33-467-41-79-13; E-mail: clg@cbs.cnrs.fr.



0006-3495/05/12/4300/10 $2.00

doi: 10.1529/biophysj.105.061697

AFM is a very powerful tool for investigating the mesoscopic and molecular organization of membranes in an aqueous environment (24–26). Supported bilayers were made of either dipalmitoylphosphatidylcholine (DPPC), a model system frequently used in peptide-lipid bilayer studies (27–29), or a binary mixture of DPPC/dioleoylphosphatidtylcholine (DOPC) under gel-fluid phase separation (26,30,31). In addition to AFM, the interactions between $P_{(\alpha)}$ and liposomes were investigated by using tryptophan (Trp) fluorescence (32–34), fluorescence anisotropy of the membrane probe 1,6-diphenyl-1,3,5-hexatriene (DPH) (35–37), and differential scanning calorimetry (DSC) (38–40).

## MATERIALS AND METHODS

### Materials

$P_{(\alpha)}$, graciously provided by Dr. Frédéric Heitz (CRBM, Montpellier) and by Dr. Thomas Billert from JenaBiosciences (Jena, Germany), was synthesized by solid phase peptide synthesis using the Fmoc strategy with AEDI-Expansin resin on a 9050 Pep synthesizer (Millipore, Watford, UK) as described (22). It is acetylated at the N-terminus and bears a cysteamide group at the C-terminus. The purity of the peptide, purified by semipreparative high pressure liquid chromatography using a Nucleosyl 300, C8, 5 $\mu$m column, 200 × 20, SFCC (Neuilly-Plaisance, France), was assessed by mass spectrometry.

Dioleoylphosphatidylcholine (DOPC) and DPPC were purchased from Avanti Polar Lipids (Alabaster, AL) and stored at −20°C under argon in chloroform/methanol 2:1 (v/v) stock solutions at a concentration of 10 mM.

### Model membranes

#### *Liposomes*

Multilamellar vesicles (MLVs) were prepared under argon, at 65°C, in phosphate buffered saline (PBS, pH 7.4) from lipid stock solutions (DPPC and DPPC/DOPC, 1:1, v/v) dried under nitrogen gas (26,41). For mixed peptide-phospholipid MLVs, $P_{(\alpha)}$ solubilized in dimethyl sulfoxide/methanol/chloroform (1:9:30, v/v/v) was added to the phospholipid solutions before drying. Corresponding large unilamellar vesicles (LUVs), with and without peptide, were obtained at the same temperature after a 10 time dilution of MLVs in the PBS buffer and extrusion through a 0.1 $\mu$m polycarbonate membrane (Avanti Polar Lipids).

#### *Supported bilayers*

Supported bilayers were prepared from LUVs as previously described (24,42). Briefly, phospholipid or mixed peptide-phospholipid LUVs were deposited on a freshly cleaved mica disk (1/2 inch diameter, Goodfellow Ltd. Huntingdon, England) enclosed in a swinney holder (Millipore, Bedford, MA) sheltered from air and allowed to fusion in a water bath for 2 h at 65°C.

The samples, always maintained in their aqueous environment, were slowly returned to room temperature, kept overnight, glued onto a steel sample puck (Digital Instruments, Santa Barbara, CA), and carefully rinsed with PBS.

### Atomic force microscopy

AFM observation of the supported bilayers was performed as previously described on a Nanoscope IIIa atomic force microscope (Digital Instruments) equipped with a fluid cell, using a J scanner (24,31). All samples were examined under PBS in contact mode. Silicon nitride cantilevers, with a 0.01 or 0.03 N/m nominal spring constant (Park Scientific Instruments, Sunnyvale, CA), were used in the experiments. The scanning force was adjusted to below 0.3 nN and readjusted for drift during image acquisition. The scan rate was adjusted between 1 and 3.5 Hz, according to the scan size. Images were obtained from at least three different samples prepared on different days with at least five macroscopically separated areas examined on each sample.

### Fluorescence studies

#### *Fluorescence polarization*

Anisotropy measurements, using DPH (Molecular Probes, Eugene, OR) as a probe, were performed on an ISS Koala spectrofluorometer (ISS, Inc., Urbana, IL) equipped with a two-cell thermostatted compartment and a magnetic stirrer as previously described (41,43). Sample temperature was monitored with a thermolinear probe directly placed into the cell compartment. DPH (0.2 mM in tetrahydrofuran) was added to the chloroform/methanol stock solution of DPPC, containing or not containing $P_{(\alpha)}$, at a molar ratio of 1 molecule of probe for 250 DPPC molecules before the drying step under nitrogen. DPH steady-state fluorescence anisotropy $r_{ss}$ was determined on LUVs according to $r_{ss} = (I_{//} + I_{\perp}G)/(I_{//} + 2I_{\perp}G)$ where $I_{//}$ and $I_{\perp}$ are the fluorescence intensities observed with the analyzing polarizer parallel and perpendicular to the polarized excitation beam. $G$, the $g$-factor, was used to correct for the unequal transmission of differently polarized light. The probe was excited at 362 nm while the emission was measured at 430 nm. Light scattering was reduced to very low levels (<1%) by the use of cutoff filters. Under all experimental conditions, individual values were the mean of at least four successive measurements which, by themselves, were the average of 20 determinations.

#### *Tryptophan fluorescence*

Tryptophan fluorescence was measured on LUVs (1 mM) in a triangular cuvette with excitation at 285 nm, using 2 nm excitation and emission slits. The fluorescence of background samples without peptide was measured and subtracted from reported data (32). A cross-oriented configuration of the polarizers ($Ex_{pol} = 90°$, $Em_{pol} = 0°$) provided maximal suppression of the scattering artifacts in spectra (34).

### Differential scanning calorimetry

The calorimetry of MLVs was done as described (24,44) on a MicroCal MC-2 calorimeter (MicroCal, Northampton, MA). For all samples a heating scan rate of 10°C/h was used. Sample runs were repeated at least three times to ensure reproducibility. The DPPC/ or DPPC/peptide MLV suspensions were in PBS buffer at a lipid concentration of 2.5 mM. The samples were degassed before use. Data analysis was done using Origin software (MicroCal Inc.).

## RESULTS

### Existence of a two-states organization for $P_{(\alpha)}$ in DPPC-supported bilayers

Low magnification AFM images of the supported bilayers under buffer showed the presence of small aggregates (*arrows*) and cracks (*arrowheads*) decorating the bilayer surface when adding 0.25 mol % $P_{(\alpha)}$ to DPPC (Fig. 1 *A*). At a higher magnification, aggregates appeared as elongated structures, ~15–25 nm in diameter and 30–60 nm in length,

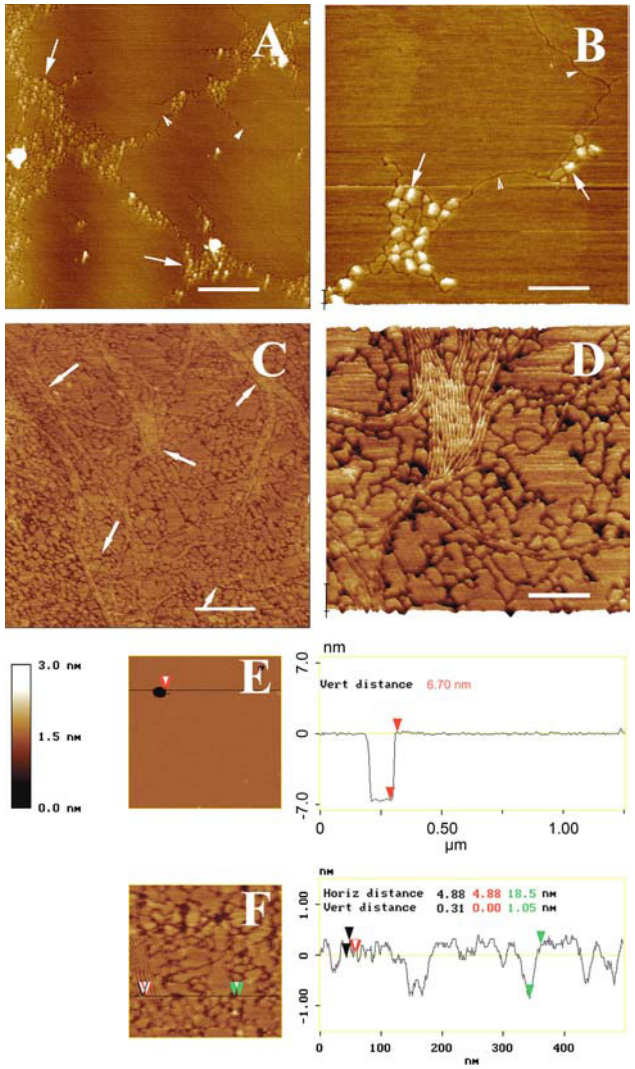


FIGURE 1 AFM imaging of DPPC bilayers at low $P_{(\alpha)}$ concentrations. (*A* and *C*) Low-magnification height image of 0.25 (*A*) and 1 (*C*) mol % $P_{(\alpha)}$ containing DPPC bilayers (*top view*, bar: 500 nm; *z* color scale: 3.0 nm); (*B* and *D*) 1 $\mu$m scan of 0.25 (*B*) and 1 (*D*) mol % $P_{(\alpha)}$-containing DPPC bilayers (3-D view, bar: 250 nm); (*E*) a virtual section of a pure DPPC bilayer region pierced by a hole; and (*F*) a virtual section of a 1 mol % $P_{(\alpha)}$-containing DPPC bilayers 500 nm scan.

protruding up to 1 nm from the bilayer (Fig. 1 *B*, *arrows*). These structures were not distributed at random but were concentrated in particular regions, bordered by cracks whose aspect and depth (0.4 ± 0.1 nm) resemble those induced by 1% gramicidin A (27). Increasing the peptide concentration to 1 mol % markedly modified the bilayer topography with the presence of thin filamentous structures, up to several micrometers in length and most often organized in bundles (Fig. 1 *C*, *arrows*). The surface was also parceled out into a multitude of small domains (20–300 nm in length) separated both by cracks and larger membrane defects of irregular shape. Decreasing the scan size (Fig. 1 *D*) showed that bundles were constituted by a homogeneous population of long single filaments, sometime curvilinear, ~5 nm in apparent diameter. The top of the filaments was between 0 and ~6 Å above the bilayer surface, a variation most likely reflecting the local mechanical properties of the bilayer (25,28,45). The depth of most interdomains defects was ~6 Å but attained ~1.1 nm for the larger defects (Fig. 1 *F*, *green arrowheads*). On the other hand, AFM imaging of supported bilayers made of pure DPPC and examined in PBS at room temperature revealed, as expected (27,28), a smooth appearance decorated with few defects (Fig. 1 *E*). The apparent height of the bilayer, determined at the edge of defects, was 6.1 ± 0.4 nm, a value which includes the thin layer of buffer sandwiched between the mica and the model membrane (26,46,47).

Bilayers prepared with 2.5 mol % $P_{(\alpha)}$ appeared highly heterogeneous at low magnification (Fig. 2 *A*) with large domains of complex shapes occupying ~1/4–1/3 of the surface according to the field examined. These large domains were made of the same long and thin filaments found in 1 mol % $P_{(\alpha)}$ samples, now tightly packed. Some single filaments traveling several hundred nm away from the bundles were also observed (Fig. 2, *B* and *C*, *arrows*). The remaining part of the sample surface was occupied by small domains surrounded by a darker matrix located 0.6 ~ 1 nm below the sample surface. As compared to the 1% samples, the size of small domains was further reduced, most of them being <50 nm in length. High resolution images suggested that the isolated filaments, preferentially surrounded by the darker matrix, could also run across both the matrix and the light small domains (Fig. 2 *D*, *arrow*). The simultaneous presence of small domains protruding from a darker matrix and of filaments strongly suggested the coexistence of two states of organization for $P_{(\alpha)}$ in DPPC samples: one inducing a local thinning of the bilayer and the other associated with the formation of supramolecular filamentous structures.

Difficulties in getting a satisfying fusion of vesicles leading to clean supported bilayers was a first consequence of increasing to 5 mol % the peptide concentration in LUV. This resulted in poor AFM imaging conditions, especially for large scans, with the presence of aggregated LUVs on the sample surface (Fig. 3 *A*, *large arrows*), often accompanied by AFM tip contamination (*thin arrows*), which explains the choice of a deflection rather than a height image. The use of smaller scans in zones between the aggregated vesicles allowed us to show that a large majority of the accessible surface of bilayers was covered by filaments (Fig. 3, *B* and *C*). This prevented the estimate of the thinnest membrane fraction. No fusion of LUVs occurred when $P_{(\alpha)}$ concentration was raised to 10 mol % (Fig. 3 *D*).

## Filaments preferentially localize in the fluid phase of mixed DPPC/DOPC-supported bilayers

As previously reported (24,30), DPPC-enriched ordered phase domains of heterogeneous shapes and size, from a few

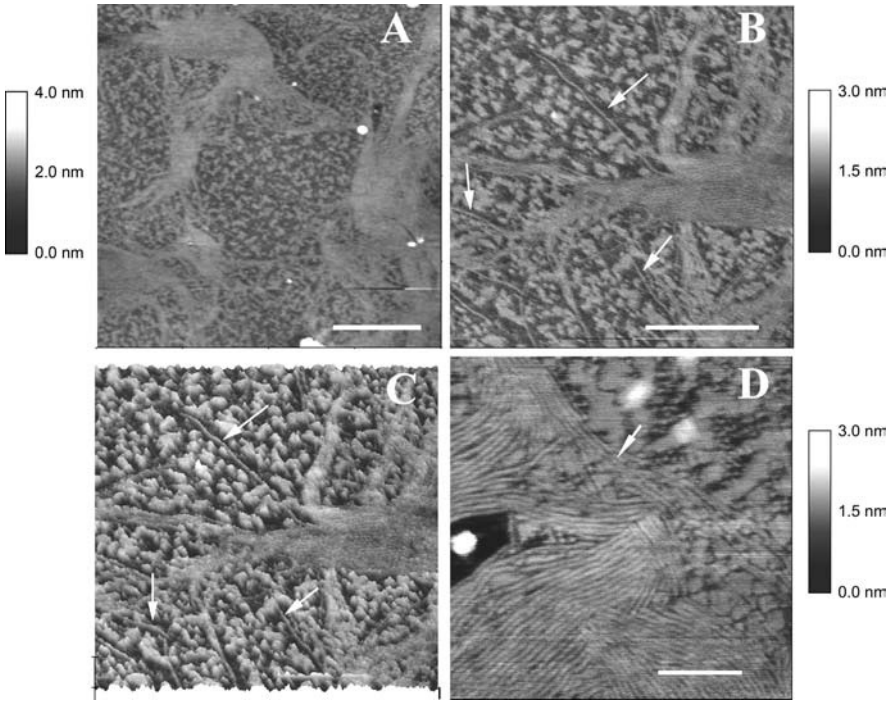


FIGURE 2 AFM imaging of 2.5 mol % $P_{(\alpha)}$-containing DPPC bilayers. Low (*A*), intermediate (*B* and *C*), and high (*D*) resolution imaging of samples under PBS buffer. (*A*, *B*, and *D*) Top view images. (*C*) A 3-D view of *B*. Bars: 1 $\mu$m (*A*), 500 nm (*B*), and 125 nm (*D*).

hundred nm up to ~20 $\mu$m, protruding by ~1 nm from the DOPC-enriched fluid matrix, characterized the supported bilayers made from DOPC/DPPC (1:1) LUVs (Fig. 4 *A*). Keeping the low magnification range, a new category of domains appeared at the membrane surface when adding 1 mol % $P_{(\alpha)}$ to the DOPC/DPPC binary mixture (Fig. 4 *B*, *arrowheads*). These domains were constituted of filaments bundles. They were exclusively observed in the DOPC fluid phase. Single curvilinear filaments several $\mu$m in length also protruded from the fluid matrix (Fig. 4 *B*, *arrows*). Three-dimensional (3-D) representation of another sample presenting defects in the bilayer allowed us to better visualize the trajectories of single filaments at the membrane surface (Fig. 4 *C*, *arrows*) and to give access to the apparent bilayer thickness of ~4.5 nm (Fig. 4 *E*). The virtual section through the bilayer also showed a filament protruding from the

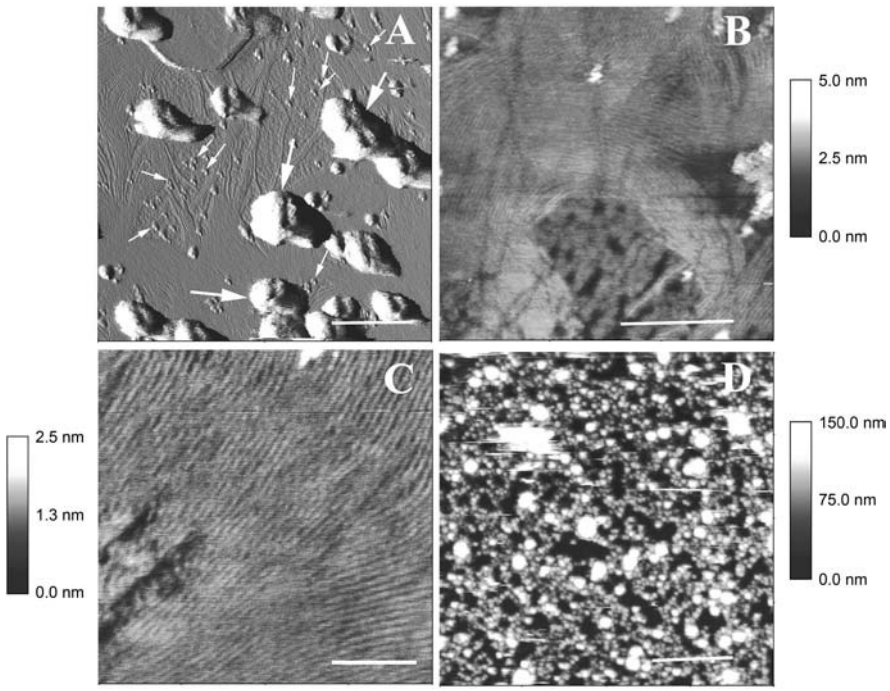


FIGURE 3 High peptide concentrations affect bilayer formation. Topography of samples at 5 mol % (*A*, *B*, and *C*) and 10 mol % (*D*) $P_{(\alpha)}$. (*A*) Low magnification imaging of a 5 mol % $P_{(\alpha)}$-containing DPPC bilayer sample showing the presence of adsorbed vesicles (deflection image, bar: 500 nm); (*B*) imaging between adsorbed vesicles (height image, bar 250 nm); (*C*) high magnification imaging of a 5 mol % $P_{(\alpha)}$ sample (height image, bar:100 nm); and (*D*) low magnification imaging of a sample made with 10 mol % $P_{(\alpha)}$. Note the large *z* color scale: 150 nm; bar: 2.5 $\mu$m.

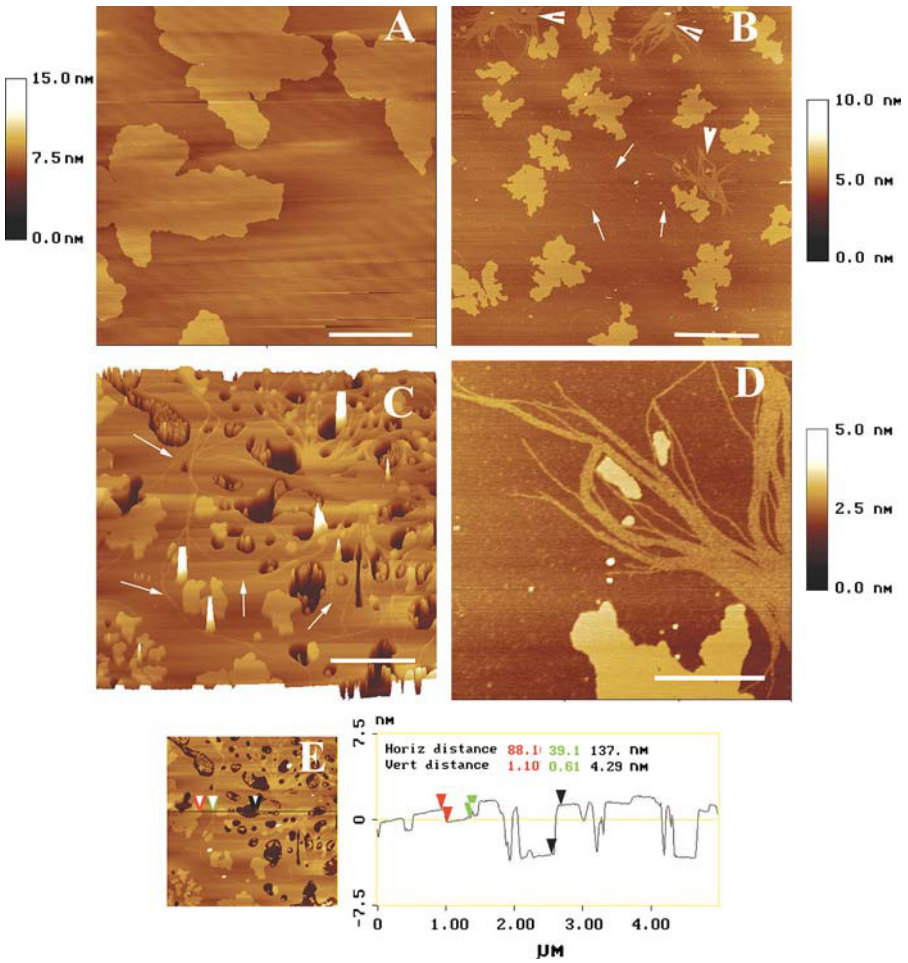


FIGURE 4 At a low concentration, peptide filaments preferentially localize in the fluid phase of DOPC/DPPC bilayers. (*A*) Low magnification imaging of DOPC/DPPC (1:1) bilayer under PBS buffer (bar: 5 $\mu$m); (*B*) low magnification imaging of DOPC/DPPC bilayers containing 1 mol % $P_{(\alpha)}$ (*top view*, bar: 2.5 $\mu$m); (*C*) 3-D view of DOPC/DPPC bilayer containing 1 mol % $P_{(\alpha)}$ at intermediate magnification (bar: 1.25 $\mu$m); (*D*) high magnification image (*top view*, bar: 500 nm); and (*E*) a virtual section of *C*.

DOPC surface by ~6 Å as compared with 1.1 nm for the DPPC domains. This difference between filaments and the DPPC domains in the emerging height from DOPC was easily detected from higher resolution scans (Fig. 4 *D*). Increasing the concentration to 5 mol % completely changed the bilayer topography (Fig. 5 *A*). The numerous filaments' bundle domains were surrounded by (Fig. 5 *B*) or rested on (*arrows* in Fig. 5, *C* and *D*) a multitude of membrane domains or fragments of undetermined phase state, giving highly contrasted 3-D images (Fig. 5 *C*). The depth of depressions and cracks between membrane domains or fragments, determined from high resolution images (Fig. 5 *D*), varied from ~1.2 to 3.5 nm, whereas isolated filaments emerged from the membrane surface by ~2 to 5 Å.

## Fluorescence studies on LUV

### *$P_{(\alpha)}$ has a limited effect on DPH anisotropy in DPPC bilayers*

DPH fluorescence anisotropy, which reports on the acyl chain packing and lipid order in membranes (36,37), is highly sensitive to the presence of transmembrane proteins and peptides in liposomes (37,48–50). As shown by Fig. 6, in which the mean ± SD anisotropy values obtained in three different experiments in the presence of peptide are plotted, 1.0 mol % $P_{(\alpha)}$ had no significant effect on DPH anisotropy in DPPC LUV. Raising to 5 mol % the $P_{(\alpha)}$ concentration in LUVs resulted in a limited but significant increase in the DPH anisotropy of the fluid phase, corresponding to an increase in the acyl chain order, without any effect on the gel phase.

### *Tryptophan fluorescence*

In $P_{(\alpha)}$, the hydrophobic and hydrophilic sequences are linked through the W-S-Q spacer to improve flexibility and to retain the integrity of the two sequences (22). For a peptide or a membrane protein, the emission $\lambda_{max}$ of a Trp residue varies 315–318 nm for a localization at or near the bilayer center to 335–340 nm if the Trp residue locates close to the surface of the bilayer (32–34). The $\lambda_{max}$ for $P_{(\alpha)}$ in buffer varied from 346 to 343 nm when increasing the peptide concentration from 5 to 20 $\mu$M. This indicated that Trp in $P_{(\alpha)}$ was partially shielded from the aqueous phase and that peptide-peptide interactions, most likely corresponding to the aggregate formation observed by AFM (23), were involved. Adding the peptide to the DPPC during the formation of LUVs resulted in a limited blue shift in $\lambda_{max}$ with

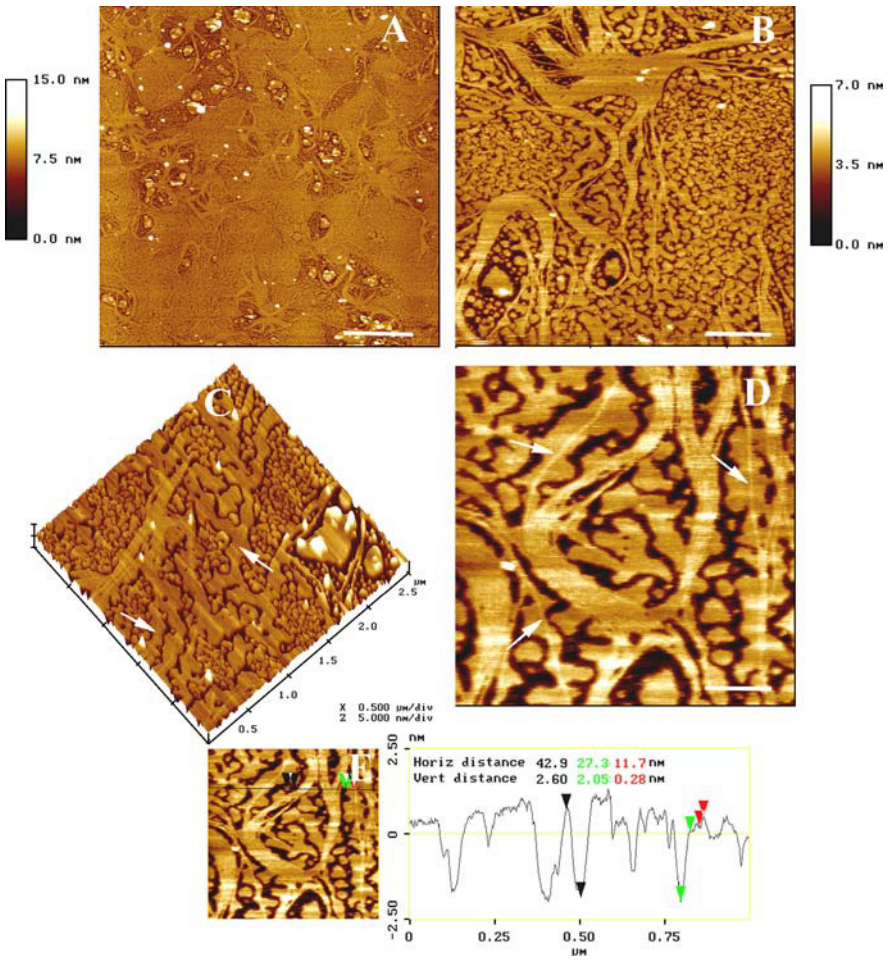


FIGURE 5 Topography of 5 mol % $P_{(\alpha)}$-containing DOPC/DPPC bilayers. (*A*), (*B*), and (*D*) the top view of bilayers at different magnifications (bars: 2 $\mu$m, 500 nm, and 200 nm, respectively). (*C*) A 3-D view of the bilayer surface at intermediate magnification. (*E*) A virtual section of (*D*).

values of 337–339 nm at 1 or 5 mol % $P_{(\alpha)}$. These values were not modified by raising the temperature to 45°C.

### *Effect of $P_{(\alpha)}$ on DPPC thermograms*

The effect of $P_{(\alpha)}$ on the thermotropic phase transition of DPPC MLVs was investigated using DSC. As shown by Fig. 7, *A* and *B*, addition of the peptide induced a concentration-dependent downward shift of moderate amplitude ($\Delta t = 0.9$°C for 5 mol % $P_{(\alpha)}$) in the main peak transition temperature. The effect was more marked for the temperature of the lamellar gel $L'_\beta$ to the lamellar ripple gel $P'_\beta$ phase pretransition which decreased by 3.4°C under the same conditions (Fig. 7 *B*). The enthalpy of the pretransition fell from 0.95 mcal/mol in controls to 0.14 mcal/mol at 5 mol % $P_{(\alpha)}$ (Fig. 7 *C*). The progressive increase in the main peak half-width (Fig. 7 *A*) suggested the existence of a peptide-dependent decrease in the cooperativity of the transition.

## DISCUSSION

The data in this study demonstrate that the cell-penetrating primary amphipathic peptide $P_{(\alpha)}$ markedly modifies the organization of supported bilayers made of DPPC in the gel phase. They strongly suggest this involves the property of $P_{(\alpha)}$ to be present in membranes under two coexisting states, one characterized by the formation of long and thin filaments lying flat on the surface, the other corresponding to peptides deeply inserted in the hydrophobic core. They show that the $P_{(\alpha)}$-induced drastic modification of the supported membrane topography also extends to DPPC/DOPC bilayers under gel-fluid phase separation. Unexpectedly, the lipid physical state of the MLVs and LUVs used for the preparation of the corresponding supported bilayers was only slightly affected by the presence of the peptide. The simultaneous two-states organization of $P_{(\alpha)}$ might be involved in its transmembrane carrier function.

### Presence of filaments in the peptide-induced reorganization of the bilayer

Between 0.25 and 5 mol %, $P_{(\alpha)}$ induced a concentration-dependent formation of both aggregates and line-shaped depression at the surface of gel phase DPPC-supported bilayers. At concentrations $\geq$1 mol %, the elongated aggregates transform into thin and very long filaments which occupied

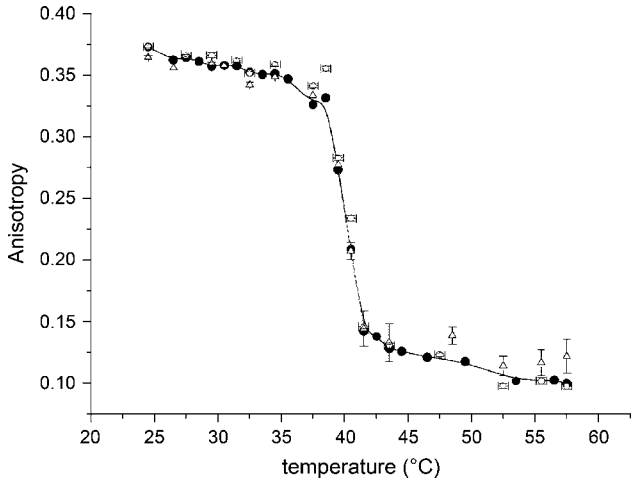


FIGURE 6 Temperature-dependent DPH fluorescence anisotropy of $P_{(\alpha)}$-containing DPPC LUV. Solid line and solid circles correspond to the values obtained for pure DPPC. Open circles correspond to the values obtained for 1 mol % $P_{(\alpha)}$ LUV. Open triangles correspond to the data obtained with 5 mol % $P_{(\alpha)}$. Each individual point is the mean ± SD of three different experiments.

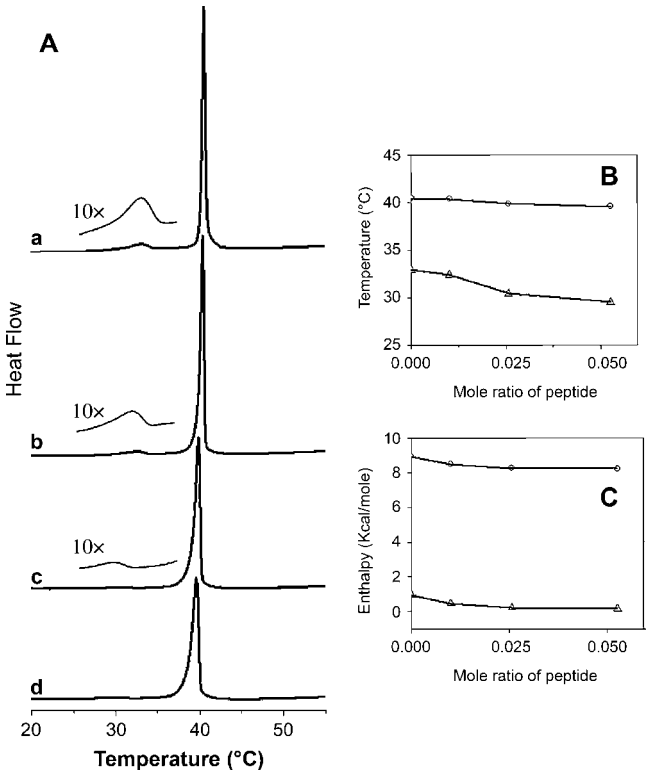


FIGURE 7 DSC heating curves of MLVs of DPPC and $P_{(\alpha)}$-DPPC mixtures. (*A*) DSC heating curves of (*a*) pure DPPC; (*b*) 1 mol % $P_{(\alpha)}$; (*c*) 2.5 mol % $P_{(\alpha)}$; and (*d*) 5 mol % $P_{(\alpha)}$. (*B*) Effect of increasing amounts of $P_{(\alpha)}$ on the peaks transition temperatures of the mixtures. (○) Main transitions. (△) Pretransitions. (*C*) Effect of increasing amounts of $P_{(\alpha)}$ on the transition enthalpies of $P_{(\alpha)}$-DPPC mixtures. (○) Total enthalpy. (△) Pretransition enthalpy.

the majority of the membrane surface at 5 mol %. This topography markedly differs from that reported, at similar concentrations, for Gramicidin A (27), transmembrane WALP peptides (28), and positively charged KALP and HALP transmembrane peptides (29), which either form small aggregates or small striated domains, or result in a fragmentation of the DPPC bilayer in small domains but do not associate two different types of membrane modification.

The organization of $P_{(\alpha)}$ filaments in bundle with line type depressions flanked by slightly protruding areas gave images that evoke the WALP studies. In these studies, lipids were assumed to account for the protruding parts and peptides for the line type depressions of striated domains (28). In pure $P_{(\alpha)}$ LB films, the peptide self-associates to form straight, thin filaments several hundred nm in length (22,23). This strongly suggests that, in our experiments, peptide or peptide-lipid complexes account for the membrane-protruding long filamentous structures. Similar filaments were also observed in mixed $P_{(\alpha)}$-phospholipids LB films, as a function of the phospholipid headgroup, the acyl chain saturation, and the lipid/peptide ratio (23). Finally with $P_{(\alpha)}$, single, long curvilinear filaments decorate the surface of both DPPC and the fluid region of DPPC/DOPC bilayers, a situation the WALP striated domains model can hardly account for.

The width of the thinnest filaments (~5 nm in apparent diameter) strongly suggests they were formed by a single row of antiparallel, side by side, packed peptides with the $\alpha$-helix principal axis oriented parallel to the membrane surface. The curvilinear shape obtained in the presence of lipids could be the result of pairs of successive peptides oriented parallel, with intercalated phospholipid headgroups to reduce electrostatic repulsion between the C-terminus. Considering the diameter of an $\alpha$-helix is ~1 nm (51), the filaments' protrusion height, up to 6 Å from the bilayer surface, indicated a peptide localization close to the polar-hydrocarbon interface.

## Simultaneous presence of peptides deeply embedded in the bilayer

Besides filaments, $P_{(\alpha)}$ induced a concentration-dependent reorganization of the bilayers into small size domains, separated by interdomain spaces 0.6–1 nm in depth. A similar localized line-shape decrease in bilayer thickness was reported for the positively charged KALP23 and Clavanin A peptides (29,52) and was attributed to the presence of ''disordered fluid-like lipids'' flanking the peptides. The hydrophobic part of $P_{(\alpha)}$ is constituted by 19 amino acids, which, assuming a length of 0.15 nm for each amino acid, gives an estimated hydrophobic length of 2.85 nm. This value is close to the value of 2.6 nm estimated for the DPPC fluid phase but is significantly lower than the 3.6 nm hydrophobic bilayer thickness of DPPC in the gel state (28).

Accordingly, our data suggest that the $\alpha$-helix part of linearly assembled peptide molecules deeply embedded in

a disordered fluid-like lipid environment accounts for a fraction of $P_{(\alpha)}$, whereas the other fraction simultaneously forms long filamentous structures lying flat on the membrane surface. We cannot ascertain if the peptide form deeply embedded in the hydrophobic core sufficiently distorts the lipid bilayer to occupy a transmembrane orientation. Such a simultaneous presence, in a single membrane, of this two-states organization for the peptide is in accordance with the data obtained on LB films where both the formation of filaments and the liquid-condensed to liquid-expanded induced transition followed the interaction of $P_{(\alpha)}$ with phospholipids (22,23). The Trp fluorescence $\lambda_{max}$ of $P_{(\alpha)}$ indicated a localization close to the surface of the bilayer in LUVs. This is not unexpected, taking into account the position of the Trp residue at the end of the peptide hydrophobic sequence and its preferential localization in the hydrophilic-hydrophobic membrane interface (29,32,33,53). No difference in Trp $\lambda_{max}$ either as a function of the $P_{(\alpha)}$ concentration in the LUVs or as a function of the temperature, corresponding to a gel or a fluid phase environment, was recorded. Most likely, this results from the fact that Trp remains anchored at the membrane interface both for the filamentous supramolecular organization and for the hydrophobic deeply embedded form.

### Supported membrane reorganization occurs without major changes in liposomes' physical state

Despite the $P_{(\alpha)}$-induced drastic alteration in the supported membranes topography, the changes in liposomes' physical state as detected by DPH anisotropy and by DSC were very limited. This was rather unexpected because the same batches of MLVs and LUVs were used to form the supported bilayers. Steady-state anisotropy of DPH is a sensitive method to detect changes in the bilayers acyl chain order upon incorporation of membrane peptides and proteins (37,49,50,54). The limited acyl chain ordering effect restricted to the fluid phase of DPPC LUVs in the presence of 5 mol % $P_{(\alpha)}$ resembles that described when adding bacteriorhodopsin to dimyristoylphosphatidylcholine (DMPC) at low protein molar ratio (lipid/protein ratio: 231) (36). This could be explained by the AFM data suggesting that most of $P_{(\alpha)}$ is present under the filamentous form, at the hydrophilic-hydrophobic interface, and by assuming that the number of lipid acyl chains involved in peptide-lipid interaction for those peptides deeply embedded in the membrane is limited by peptide propensity to self-assemble. Such a possibility is supported by electrospray mass spectrometry studies indicating the formation of (1:1) DMPC/$P_{(\alpha)}$ noncovalent complexes (55) while 16–18 molecules of phosphatidylcholine are required to surround a transmembrane $\propto$-helical peptide. It is worth noting that magainin or indolicin, when oriented parallel to the bilayer surface, have no influence on DPH polarization whereas they change it as soon as they adopt a transmembrane orientation (50).

The same reasons could also account for the DSC results. The marked effect on the pretransition peak, the moderate decrease in the main peak transition temperature associated with a broadening of its half-width, and the limited effect on the transition enthalpy are in accordance with a predominant localization of $P_{(\alpha)}$ at the interfacial region where it behaves like a Group II protein on an uncharged surface (38,40,56). This behavior differs from that of transmembrane peptides like $K_2GL_nK_2A$-amide (38), Ac-$K_2L_{24}K_2$-amide (57), and the WALP23, KALP23, and HALP23 series (29), which belong to the Group III proteins. It has to be noticed that for these last peptide series, 2 mol % peptide induces $<10\%$ decrease in the transition enthalpy. Considering that only a fraction of $P_{(\alpha)}$ molecules is deeply embedded in the membrane hydrophobic core and that, furthermore, these peptides spontaneously assemble, it can be conceived that the relative number of lipid acyl chains involved in lipid-peptide interactions become too low for a decrease in the main peak enthalpy to be detected.

Existence of the two $P_{(\alpha)}$ populations could explain how $P_{(\alpha)}$ induces marked changes in the supported bilayer topography whereas corresponding changes in the liposomes membrane physical state are only very limited. The presence at the bilayer surface of very long filaments, several micrometers in length, however, strongly suggests that the membrane modification occurring in vesicles can be amplified in supported bilayers. Considering the diameter of a single LUV ($\sim$100 nm), the size of these filaments, which even at 10 mol % $P_{(\alpha)}$ were never observed at the vesicles surface, implies they were formed after the vesicles' fusion step. This strongly suggests that large membrane reorganization, likely also involving the deeply embedded peptides forming the thinner zones, might occur when passing from a spherical to a flat bilayer configuration.

## CONCLUSION

The results of this study show the unexpected ability of a primary amphipathic CPP $P_{(\alpha)}$ to simultaneously form long filamentous structures lying flat on the surface and peptide-enriched domains embedded in the hydrophobic core of membranes. This brings strong support to the concept of an equilibrium between coexisting transmembrane and non-transmembrane forms of $\alpha$-helical peptides with hydrophobic sequences of length close enough to that of the lipid core (32,58–60). The duality of $P_{(\alpha)}$ interaction with membranes resembles the mechanism described for most antimicrobial peptides. For these peptides, which bear a positive charge, are hydrophobic, and usually membrane active, molecular self-assembly is believed to play a key role in the membrane disruption properties (61–63). The different models involve a reorientation of at least a part of the concentrated peptides that lie on the membrane surface (surface state, S) toward a transbilayer insertion (insertion state, I). The S $\leftrightarrow$ I transition depends on the peptide concentration and lipid

composition (64). It was proposed that a subtle equilibrium exists between the adsorbed and inserted peptide, which might provide a control mechanism for reversible insertion and pore formation (65). This suggests that translocation of cargoes across cell membranes by primary amphipathic CPPs may use mechanisms close to those of antimicrobial peptides.

This work was supported by European Union grant QLK2-CT-2001-01451.

## REFERENCES


1. Lindgren, M., M. Hallbrink, A. Prochiantz, and U. Langel. 2000. Cell-penetrating peptides. *Trends Pharmacol. Sci.* 21:99–103.
2. Prochiantz, A. 1996. Getting hydrophilic compounds into cells: lessons from homeopeptides. *Curr. Opin. Neurobiol.* 6:629–634.
3. Prochiantz, A. 2000. Messenger proteins: homeoproteins, TAT and others. *Curr. Opin. Cell Biol.* 12:400–406.
4. Dietz, G. P., and M. Bahr. 2004. Delivery of bioactive molecules into the cell: the Trojan horse approach. *Mol. Cell. Neurosci.* 27:85–131.
5. Drin, G., S. Cottin, E. Blanc, A. R. Rees, and J. Temsamani. 2003. Studies on the internalization mechanism of cationic cell-penetrating peptides. *J. Biol. Chem.* 278:31192–31201.
6. Richard, J. P., K. Melikov, E. Vives, C. Ramos, B. Verbeure, M. J. Gait, L. V. Chernomordik, and B. Lebleu. 2003. Cell-penetrating peptides. A reevaluation of the mechanism of cellular uptake. *J. Biol. Chem.* 278:585–590.
7. Trehin, R., and H. P. Merkle. 2004. Chances and pitfalls of cell penetrating peptides for cellular drug delivery. *Eur. J. Pharm. Biopharm.* 58:209–223.
8. Thoren, P. E., D. Persson, E. K. Esbjorner, M. Goksor, P. Lincoln, and B. Norden. 2004. Membrane binding and translocation of cell-penetrating peptides. *Biochemistry.* 43:3471–3489.
9. Binder, H., and G. Lindblom. 2003. Charge-dependent translocation of the Trojan peptide penetratin across lipid membranes. *Biophys. J.* 85:982–995.
10. Terrone, D., W. S. S. Leung, L. Roudaia, and J. R. Silvius. 2003. Penetratin and related cell-penetrating cationic peptides can translocate across lipid bilayers in the presence of a transbilayer potential. *Biochemistry.* 42:13787–13799.
11. Morris, M. C., P. Vidal, L. Chaloin, F. Heitz, and G. Divita. 1997. A new peptide vector for efficient delivery of oligonucleotides into mammalian cells. *Nucleic Acids Res.* 25:2730–2736.
12. Morris, M. C., L. Chaloin, F. Heitz, and G. Divita. 2000. Translocating peptides and proteins and their use for gene delivery. *Curr. Opin. Biotechnol.* 11:461–466.
13. Simeoni, F., M. C. Morris, F. Heitz, and G. Divita. 2003. Insight into the mechanism of the peptide-based gene delivery system MPG: implications for delivery of siRNA into mammalian cells. *Nucleic Acids Res.* 31:2717–2724.
14. Kalderon, D., W. D. Richardson, A. F. Markham, and A. E. Smith. 1984. Sequence requirements for nuclear location of simian virus 40 large-T antigen. *Nature.* 311:33–38.
15. Goldfarb, D. S., J. Gariepy, G. Schoolnik, and R. D. Kornberg. 1986. Synthetic peptides as nuclear localization signals. *Nature.* 322:641–644.
16. Chaloin, L., P. Vidal, A. Heitz, N. Van Mau, J. Mery, G. Divita, and F. Heitz. 1997. Conformations of primary amphipathic carrier peptides in membrane mimicking environments. *Biochemistry.* 36:11179–11187.
17. Chaloin, L., P. Vidal, P. Lory, J. Mery, N. Lautredou, G. Divita, and F. Heitz. 1998. Design of carrier peptide-oligonucleotide conjugates with rapid membrane translocation and nuclear localization properties. *Biochem. Biophys. Res. Commun.* 243:601–608.
18. Vidal, P., M. C. Morris, L. Chaloin, F. Heitz, and G. Divita. 1997. New strategy for RNA vectorization in mammalian cells. Use of a peptide vector. *C. R. Acad. Sci. III.* 320:279–287.
19. Vidal, P., L. Chaloin, A. Heitz, N. Van Mau, J. Mery, G. Divita, and F. Heitz. 1998. Interactions of primary amphipathic vector peptides with membranes. Conformational consequences and influence on cellular localization. *J. Membr. Biol.* 162:259–264.
20. Van Mau, N., V. Vie, L. Chaloin, E. Lesniewska, F. Heitz, and C. Le Grimellec. 1999. Lipid-induced organization of a primary amphipathic peptide: a coupled AFM-monolayer study. *J. Membr. Biol.* 167:241–249.
21. Vie, V., N. Van Mau, L. Chaloin, E. Lesniewska, C. Le Grimellec, and F. Heitz. 2000. Detection of peptide-lipid interactions in mixed monolayers, using isotherms, atomic force microscopy, and Fourier transform infrared analyses. *Biophys. J.* 78:846–856.
22. Deshayes, S., T. Plenat, G. Aldrian-Herrada, G. Divita, C. Le Grimellec, and F. Heitz. 2004. Primary amphipathic cell-penetrating peptides: structural requirements and interactions with model membranes. *Biochemistry.* 43:7698–7706.
23. Plenat, T., S. Deshayes, S. Boichot, P. E. Milhiet, R. B. Cole, F. Heitz, and C. Le Grimellec. 2004. Interaction of primary amphipathic cell-penetrating peptides with phospholipid-supported monolayers. *Langmuir.* 20:9255–9261.
24. Giocondi, M. C., V. Vie, E. Lesniewska, P. E. Milhiet, M. Zinke Allmang, and C. Le Grimellec. 2001. Phase topology and growth of single domains in lipid bilayers. *Langmuir.* 17:1653–1659.
25. Milhiet, P. E., M. C. Giocondi, and C. Le Grimellec. 2003. AFM imaging of lipid domains in model membranes. *ScientificWorldJournal.* 3:59–74.
26. Giocondi, M. C., and C. Le Grimellec. 2004. Temperature dependence of the surface topography in dimyristoylphosphatidylcholine/distearoylphosphatidylcholine multibilayers. *Biophys. J.* 86:2218–2230.
27. Mou, J., D. M. Czajkowsky, and Z. Shao. 1996. Gramicidin A aggregation in supported gel state phosphatidylcholine bilayers. *Biochemistry.* 35:3222–3226.
28. Rinia, H. A., R. A. Kik, R. A. Demel, M. M. Snel, J. A. Killian, J. P. van Der Eerden, and B. de Kruijff. 2000. Visualization of highly ordered striated domains induced by transmembrane peptides in supported phosphatidylcholine bilayers. *Biochemistry.* 39:5852–5858.
29. Rinia, H. A., J. W. P. Boots, D. T. S. Rijkers, R. A. Kik, M. M. E. Snel, R. A. Demel, J. A. Killian, J. van der Eerden, and B. de Kruijff. 2002. Domain formation in phosphatidylcholine bilayers containing transmembrane peptides: specific effects of flanking residues. *Biochemistry.* 41:2814–2824.
30. Berquand, A., M. P. Mingeot-Leclercq, and Y. F. Dufrene. 2004. Real-time imaging of drug- membrane interactions by atomic force microscopy. *Biochim. Biophys. Acta.* 1664:198–205.
31. Boichot, S., U. Krauss, T. Plenat, R. Rennert, P. E. Milhiet, A. Beck-Sickinger, and C. Le Grimellec. 2004. Calcitonin-derived carrier peptide plays a major role in the membrane localization of a peptide-cargo complex. *FEBS Lett.* 569:346–350.
32. Ren, J., S. Lew, Z. Wang, and E. London. 1997. Transmembrane orientation of hydrophobic alpha-helices is regulated both by the relationship of helix length to bilayer thickness and by the cholesterol concentration. *Biochemistry.* 36:10213–10220.
33. Wimley, W. C., and S. H. White. 1996. Experimentally determined hydrophobicity scale for proteins at membrane interfaces. *Nat. Struct. Biol.* 3:842–848.
34. Ladokhin, A. S., S. Jayasinghe, and S. H. White. 2000. How to measure and analyse tryptophan fluorescence in membranes properly, and why bother? *Anal. Biochem.* 285:235–245.
35. Lentz, B. R., Y. Barenholz, and T. E. Thompson. 1976. Fluorescence depolarization studies of phase transitions and fluidity in phospholipid bilayers. 2 Two-component phosphatidylcholine liposomes. *Biochemistry.* 15:4529–4537.
36. Heyn, M. P. 1979. Determination of lipid order parameters and rotational correlation times from fluorescence depolarization experiments. *FEBS Lett.* 108:359–364.

37. Jahnig, F., H. Vogel, and L. Best. 1982. Unifying description of the effect of membrane proteins on lipid order. Verification for the melittin/dimyristoylphosphatidylcholine system. *Biochemistry*. 21: 6790–6798.

38. Papahadjopoulos, D., M. Moscarello, E. H. Eylar, and T. Isac. 1975. Effects of proteins on thermotropic phase transitions of phospholipid membranes. *Biochim. Biophys. Acta*. 401:317–335.

39. Morrow, M. R., J. C. Huschilt, and J. H. Davis. 1985. Simultaneous modeling of phase and calorimetric behavior in an amphiphilic peptide/phospholipid model membrane. *Biochemistry*. 24:5396–5406.

40. McElhaney, R. N. 1986. Differential scanning calorimetric studies of lipid-protein interactions in model membrane systems. *Biochim. Biophys. Acta*. 864:361–421.

41. el Yandouzi, E. H., and C. Le Grimellec. 1993. Effect of cholesterol oxidase treatment on physical state of renal brush border membranes: evidence for a cholesterol pool interacting weakly with membrane lipids. *Biochemistry*. 32:2047–2052.

42. Giocondi, M. C., P. E. Milhiet, P. Dosset, and C. Le Grimellec. 2004. Use of cyclodextrin for AFM monitoring of model raft formation. *Biophys. J*. 86:861–869.

43. Le Grimellec, C., M. C. Giocondi, B. Carriere, S. Carriere, and J. Cardinal. 1982. Membrane fluidity and enzyme activities in brush border and basolateral membranes of the dog kidney. *Am. J. Physiol*. 242:F246–F253.

44. Milhiet, P. E., M. C. Giocondi, and C. Le Grimellec. 2002. Cholesterol is not crucial for the existence of microdomains in kidney brush-border membrane models. *J. Biol. Chem*. 277:875–878.

45. Shao, Z., J. Mou, D. M. Czajkowksy, J. Yang, and J. Y. Yuan. 1996. Biological atomic force microscopy: what is achieved & what is needed. *Adv. Phys*. 45:1–86.

46. Wack, D. C., and W. W. Webb. 1989. Synchrotron x-ray study of the modulated lamellar phase P beta ′ in the lecithin-water system. *Phys. Rev. A*. 40:2712–2730.

47. Johnson, S. J., T. M. Bayerl, D. C. McDermott, G. W. Adam, A. R. Rennie, R. K. Thomas, and E. Sackmann. 1991. Structure of an adsorbed dimyristoylphosphatidylcholine bilayer measured with specular reflection of neutrons. *Biophys. J*. 59:289–294.

48. Gomez-Fernandez, J. C., F. M. Goni, D. Bach, C. Restall, and D. Chapman. 1979. Protein–lipid interactions. A study of (Ca2+-Mg2+)ATPase reconstituted with synthetic phospholipids. *FEBS Lett*. 98:224–228.

49. Petri, W. A. Jr., R. Pal, Y. Barenholz, and R. R. Wagner. 1981. Fluorescence studies of dipalmitoylphosphatidylcholine vesicles reconstituted with the glycoprotein of vesicular stomatitis virus. *Biochemistry*. 20:2796–2800.

50. Zhao, H., J. P. Mattila, J. M. Holopainen, and P. K. Kinnunen. 2001. Comparison of the membrane association of two antimicrobial peptides, magainin 2 and indolicidin. *Biophys. J*. 81:2979–2991.

51. Reithmeier, R. A. 1995. Characterization and modeling of membrane proteins using sequence analysis. *Curr. Opin. Struct. Biol*. 5:491–500.

52. Van Kan, E. J. M., D. N. Ganchev, M. M. E. Snel, V. Chupin, A. Van der Bent, and B. De Kruijff. 2003. The peptide antibiotic clavanin A interacts strongly and specifically with lipid bilayers. *Biochemistry*. 42:11366–11372.

53. Wimley, W. C., and S. H. White. 2000. Determining the membrane topology of peptides by fluorescence quenching. *Biochemistry*. 39: 161–170.

54. Lentz, B. R., K. W. Clubb, D. R. Alford, M. Hochli, and G. Meissner. 1985. Phase behavior of membranes reconstituted from dipentadecanoylphosphatidylcholine and the Mg2+-dependent, Ca2+-stimulated adenosinetriphosphatase of sarcoplasmic reticulum: evidence for a disrupted lipid domain surrounding protein. *Biochemistry*. 24:433–442.

55. Li, Y., F. Heitz, C. Le Grimellec, and R. B. Cole. 2005. Fusio-peptide-phospholipid noncovalent interactions as observed by nanoelectrospray FTICR-MS. *Anal. Chem*. 77:1556–1565.

56. Prenner, E. J., R. N. Lewis, L. H. Kondejewski, R. S. Hodges, and R. N. McElhaney. 1999. Differential scanning calorimetric study of the effect of the antimicrobial peptide gramicidin S on the thermotropic phase behavior of phosphatidylcholine, phosphatidylethanolamine and phosphatidylglycerol lipid bilayer membranes. *Biochim. Biophys. Acta*. 1417:211–223.

57. Pare, C., M. Lafleur, F. Liu, R. N. Lewis, and R. N. McElhaney. 2001. Differential scanning calorimetry and (2)H nuclear magnetic resonance and Fourier transform infrared spectroscopy studies of the effects of transmembrane alpha-helical peptides on the organization of phosphatidylcholine bilayers. *Biochim. Biophys. Acta*. 1511:60–73.

58. Gil, T., J. H. Ipsen, O. G. Mouritsen, M. C. Sabra, M. M. Sperotto, and M. J. Zuckermann. 1998. Theoretical analysis of protein organization in lipid membranes. *Biochim. Biophys. Acta*. 1376:245–266.

59. Killian, J. A. 1998. Hydrophobic mismatch between proteins and lipids in membranes. *Biochim. Biophys. Acta*. 1376:401–415.

60. Jensen, M. O., and O. G. Mouritsen. 2004. Lipids do influence protein function: the hydrophobic matching hypothesis revisited. *Biochim. Biophys. Acta*. 1666:205–226.

61. Epand, R. M., Y. Shai, J. P. Segrest, and G. M. Anantharamaiah. 1995. Mechanisms for the modulation of membrane bilayer properties by amphipathic helical peptides. *Biopolymers*. 37:319–338.

62. Matsuzaki, K. 1998. Magainins as paradigm for the mode of action of pore forming polypeptides. *Biochim. Biophys. Acta*. 1376:391–400.

63. Shai, Y. 2002. Mode of action of membrane active antimicrobial peptides. *Biopolymers*. 66:236–248.

64. Heller, W. T., A. J. Waring, R. I. Lehrer, and H. W. Huang. 1998. Multiple states of beta-sheet peptide protegrin in lipid bilayers. *Biochemistry*. 37:17331–17338.

65. Zuckermann, M. J., and T. Heimburg. 2001. Insertion and pore formation driven by adsorption of proteins onto lipid bilayer membrane-water interfaces. *Biophys. J*. 81:2458–2472.